

Facile synthesis of $\text{Ag}_3\text{PO}_4/\text{C}_3\text{N}_4$ composites with improved visible light photocatalytic activity

Bo Chai,^{a)} Fangyuan Zou, and Wenjie Chen

School of Chemical and Environmental Engineering, Wuhan Polytechnic University, Wuhan 430023, People's Republic of China

(Received 8 January 2015; accepted 17 March 2015)

The $\text{Ag}_3\text{PO}_4/\text{C}_3\text{N}_4$ composites with improved photocatalytic activity were prepared by a facile *in situ* deposition of Ag_3PO_4 particles on the surface of C_3N_4 sheets and characterized by x-ray diffraction, field emission scanning electron microscopy, transmission electron microscopy, x-ray photoelectron spectroscopy, UV-vis diffuse reflectance absorption spectra, Fourier transform infrared spectra, and photoluminescence spectra. The photocatalytic degradation of Rhodamine B (RhB) over the $\text{Ag}_3\text{PO}_4/\text{C}_3\text{N}_4$ composites was investigated and optimized, indicating that the optimal amount of Ag_3PO_4 in the composites was 90 wt%. The remarkably improved photocatalytic activity of $\text{Ag}_3\text{PO}_4/\text{C}_3\text{N}_4$ composites could be attributed to the effective separation of photogenerated charge carriers. The photoelectrochemical measurements confirmed that the charge separation efficiency was improved for the formation of composites. Moreover, the tests of radical scavengers demonstrated that h^+ and $\cdot\text{O}_2^-$ were the main active species for the degradation of RhB.

I. INTRODUCTION

Semiconductor photocatalysis driven by visible light has been paid more attention in the past few decades because of its potential applications in environmental remediation and hydrogen energy production by utilization of solar light energy.^{1,2} Design and synthesis of novel visible-light-responsive photocatalysts are still the focus in this field.^{3–5} In recent years, silver orthophosphate (Ag_3PO_4) and carbon nitrides (C_3N_4) have been respectively reported as visible-light-active photocatalysts for the photodecomposition of organic compounds.^{6–10} However, bare Ag_3PO_4 is prone to photocorrosion and decomposing to weakly active Ag during the photocatalytic reaction process, which could deteriorate its photocatalytic activity.^{11,12} On the other hand, the photocatalytic performance of pristine C_3N_4 is limited owing to the high recombination rate of photogenerated electron–hole pairs.¹³ Therefore, it is necessary to develop an efficient strategy to overcome these drawbacks of single Ag_3PO_4 or C_3N_4 as photocatalysts. Coupling two semiconductors to form composites is considered as an effective approach toward improving the separation efficiency of charge carriers, and then enhancing the photocatalytic activity and stability.^{14–24} In this case, various Ag_3PO_4 -based and C_3N_4 -based coupled systems have been explored such as $\text{AgBr}/\text{Ag}_3\text{PO}_4$,¹⁴ $\text{Ag}_3\text{PO}_4/\text{TiO}_2$,¹⁵ $\text{Ag}_3\text{PO}_4/\text{ZnO}$,¹⁶

$\text{Ag}_3\text{PO}_4/\text{SnO}_2$,¹⁷ $\text{Bi}_2\text{MoO}_6/\text{Ag}_3\text{PO}_4$,¹⁸ $\text{Bi}_2\text{WO}_6/\text{Ag}_3\text{PO}_4$,¹⁹ $\text{TiO}_2/\text{C}_3\text{N}_4$,²⁰ $\text{ZnO}/\text{C}_3\text{N}_4$,²¹ $\text{ZnWO}_4/\text{C}_3\text{N}_4$,²² $\text{CdS}/\text{C}_3\text{N}_4$,²³ $\text{BiOBr}/\text{C}_3\text{N}_4$,²⁴ and so on. The photocatalytic reaction results indicated that the formation of composites could enhance the photocatalytic activity of Ag_3PO_4 or C_3N_4 .

According to previous reports,^{25,26} the conduction band (CB) and valence band (VB) potentials of Ag_3PO_4 [~ 0.24 and ~ 2.69 eV versus normal hydrogen electrode (NHE), respectively] are both lower than those of C_3N_4 (~ -1.12 and ~ 1.73 eV versus NHE, respectively). This staggered energy band structure favors the separation of photogenerated charge carriers when Ag_3PO_4 combines with C_3N_4 to form composites. Very recently, several groups have reported the synthesis of $\text{Ag}_3\text{PO}_4/\text{C}_3\text{N}_4$ composites with enhanced photocatalytic activity and stability.^{25,27–31} As a promising hybrid material for photocatalysis, the exploration of $\text{Ag}_3\text{PO}_4/\text{C}_3\text{N}_4$ composites still has a long way to go, especially through a facile, environmentally friendly, and economical method. In this work, $\text{Ag}_3\text{PO}_4/\text{C}_3\text{N}_4$ composites were prepared by a facile *in situ* deposition of Ag_3PO_4 particles on the surface of C_3N_4 sheets at room temperature and applied into photocatalytic degradation of Rhodamine B (RhB) solution under visible light irradiation. Remarkably, enhanced photocatalytic activity was achieved compared with single Ag_3PO_4 or C_3N_4 . Moreover, the effect of mass ratios of Ag_3PO_4 in the $\text{Ag}_3\text{PO}_4/\text{C}_3\text{N}_4$ composites on photocatalytic activity was investigated comparatively. Compared with the previous reports, our work provides some new and meaningful results on the radical scavenger and photoelectric conversion measurement experiments, which

Contributing Editor: Xiaobo Chen

^{a)}Address all correspondence to this author.

e-mail: willycb@163.com

DOI: 10.1557/jmr.2015.91

indicate the main species in the catalytic system and support the possible photocatalytic mechanism.

II. EXPERIMENTAL SECTION

A. Materials preparation

C_3N_4 was synthesized by thermal treatment of 5 g urea (AR, Sinopharm Chemical Reagent Co. Ltd., China) in an alumina crucible with a cover. After being dried at 80 °C for 12 h, the urea was heated to 500 °C and held for 3 h with a heating rate of 5 °C min⁻¹. The resultant light yellow powders were collected for use without further treatment.

$\text{Ag}_3\text{PO}_4/\text{C}_3\text{N}_4$ composites were prepared as follows: an appropriate amount of C_3N_4 was added into 30 mL of deionized water with sonicating for 30 min to make C_3N_4 dispersion totally. 0.26 g of AgNO_3 was dissolved in 1.5 mL concentrated ammonia to form a transparent silver-ammino complex solution. Afterward, the later solution was introduced into the former one and stirred for 30 min before the addition of 0.183 g $\text{Na}_2\text{HPO}_4 \cdot 12\text{H}_2\text{O}$. The pH value of a mixture was adjusted to 7.30 by 0.1 M HNO_3 solution. The suspensions were stirred for 4 h in the dark at room temperature. The resultant powders were washed with ethanol and deionized water several times, dried in a vacuum at 60 °C for 12 h. For comparison, a series of $\text{Ag}_3\text{PO}_4/\text{C}_3\text{N}_4$ composites with different theoretical mass ratios of Ag_3PO_4 (from 50 to 92 wt%) in the composites were fabricated by changing C_3N_4 amounts. Similarly, the pristine Ag_3PO_4 was also prepared by following the same procedure as above except the addition of C_3N_4 .

B. Material characterization

The samples were characterized by x-ray diffraction (XRD) patterns using a Bruker D8 Advance x-ray diffractometer with Cu K α irradiation ($\lambda = 0.154178$ nm) at 40 kV and 40 mA. The morphology of samples was investigated by a JSM-6700F microscope (Japan Electron Optics Laboratory Co., Ltd., Japan). The transmission electron microscopy (TEM) measurement was conducted using a JEOL JEM 2100F microscope (Japan Electron Optics Laboratory Co., Ltd., Japan) working at 200 kV. The x-ray photoelectron spectroscopy (XPS) measurement was performed on a VG Multilab 2000 (Thermo Electron Corporation, USA) with Al K α source operation at 300 W. The UV-vis diffuse reflectance absorption spectra (DRS) were obtained by a Shimadzu UV-3600 spectrophotometer (Shimadzu Corporation, Japan) equipped with an integrating sphere using BaSO_4 as the reference sample. The Fourier transform infrared spectra (FTIR) spectra of samples were recorded on a Thermo Nicolet Avatar 360 spectrometer using conventional KBr pellets. The photoluminescence (PL) spectra were measured at room temperature on a varian cary eclipse

fluorescence spectrophotometer with the excitation wavelength at 340 nm.

C. Photocatalytic activity measurement

The photocatalytic activities of $\text{Ag}_3\text{PO}_4/\text{C}_3\text{N}_4$ composites were evaluated by the degradation of RhB aqueous solution under visible light irradiation. 50 mg of photocatalysts were added into 100 mL of RhB solution with the initial concentration of 1.0×10^{-5} mol·L⁻¹. A 500 W xenon lamp (Changzhou Yuyu Electro-Optical Device Co. Ltd., China) with a 420 nm cutoff filter provided visible light irradiation. Prior to irradiations, the suspensions were magnetically stirred in the dark for 30 min to ensure the establishment of an adsorption-desorption equilibrium. At given irradiation time intervals, about 4 mL of the suspensions were collected and then centrifuged at 10,000 rpm for 10 min to remove the photocatalysts. The TU-1810 spectrophotometer (Beijing Purkinje General Instrument Co. Ltd., China) was used to measure the concentration changes of RhB solution with the wave length of 554 nm.

D. Photoelectric conversion measurement

The transient photocurrent responses and electrochemical impedance spectra (EIS) were performed on an electrochemical system (CHI 660E, China). A standard three-electrode cell with a working electrode (as-prepared photocatalysts), a platinum plate as the counter electrode, and Ag/AgCl electrode (saturated KCl) as the reference electrode were used in the photoelectric studies. 0.1 mol L⁻¹ Na_2SO_4 was used as the electrolyte solution. For the preparation of working electrodes, a certain amount of photocatalysts were suspended in 1 mL ethanol with 0.1 mL Nafion aqueous solution (5 wt%), the mixtures were ultrasonically scattered for 30 min to form a homogeneous solution. Then, 0.1 mL solution was dropped on the indium tin oxide (ITO) glass (1 cm × 1 cm). After evaporation of the ethanol in air, the catalyst was attached on the ITO glass surface. Photocurrent and EIS tests were irradiated under visible light through a 300 W Xe lamp with a 420 nm cut-off filter.

III. RESULTS AND DISCUSSION

The XRD patterns of C_3N_4 , Ag_3PO_4 , and 90 wt% $\text{Ag}_3\text{PO}_4/\text{C}_3\text{N}_4$ composite are shown in Fig. 1. As could be seen from the diffraction pattern of C_3N_4 , there is a broad peak at about 27.6°, which is characteristic peak of C_3N_4 corresponding to the (002) plane.²⁶ As for pristine Ag_3PO_4 , all of the diffraction peaks could be well indexed to the cubic phase of Ag_3PO_4 (JCPDS, No. 06-0505), in agreement with previous reports.^{27,28} The intense diffraction peaks of Ag_3PO_4 indicate that the as-prepared sample would be well crystallized. In addition, the 90 wt% $\text{Ag}_3\text{PO}_4/\text{C}_3\text{N}_4$ composite exhibits a similar XRD pattern

to that of bare Ag_3PO_4 . No diffraction peak assigning to C_3N_4 is observed, which may be due to the relatively low diffraction intensity of C_3N_4 in the composite.

Figures 2(a)–2(c) show the field emission scanning electron microscopy (FESEM) images of C_3N_4 , Ag_3PO_4 , and 90 wt% $\text{Ag}_3\text{PO}_4/\text{C}_3\text{N}_4$ composite. It is seen that C_3N_4 presents obvious two-dimensional (2D) lamellar structure, which is consistent with the previous report.²⁶ Pristine Ag_3PO_4 exhibits irregular particle morphology with the diameters of 100–500 nm together with smooth surface. For the 90 wt% $\text{Ag}_3\text{PO}_4/\text{C}_3\text{N}_4$ composite, it is

constituted with the layer-like C_3N_4 and granular Ag_3PO_4 . The TEM image [Fig. 2(d)] of 90 wt% $\text{Ag}_3\text{PO}_4/\text{C}_3\text{N}_4$ further confirms that Ag_3PO_4 particles are intimately attached on the surface of C_3N_4 , in agreement with the FESEM observation.

The XPS measurement was performed to determine the chemical composition and valence state of various species. The peak positions in all of the XPS spectra are calibrated with C 1s at 284.6 eV. Figure 3(a) displays the XPS survey spectrum of 90 wt% $\text{Ag}_3\text{PO}_4/\text{C}_3\text{N}_4$ composite. As expected, it contains Ag, P, O, C, and N elements. The peaks [Fig. 3(b)] with a binding energy of 368.5 and 374.5 eV in the high resolution XPS spectrum of Ag 3d are assigned to Ag^{3+} and Ag^{2+} , indicating the existence of Ag^+ in the composite. The XPS peak of P 2p is found at 133.3 eV [Fig. 3(c)], which could be attributed to P^{5+} in PO_4^{3-} .³² The O 1s XPS spectrum illustrated in Fig. 3(d) could be deconvoluted into two peaks at 530.6 and 531.6 eV. The former corresponds to the crystal lattice oxygen of Ag_3PO_4 ,³² the latter could be derived from the chemisorbed oxygen of surface hydroxyls or incompletely reacted oxygen-containing intermediates during the preparation of C_3N_4 .¹⁰ The C 1s [Fig. 3(e)] XPS spectra have two distinct peaks at 284.6 and 288.2 eV. The peak at 288.2 eV is identified as sp^2 -bonded carbon (N=C=N). The peak located at 284.6 eV could be assigned to adventitious carbon and graphitic carbon.^{10,26} As shown in Fig. 3(e), the N 1s peaks at 398.5 and

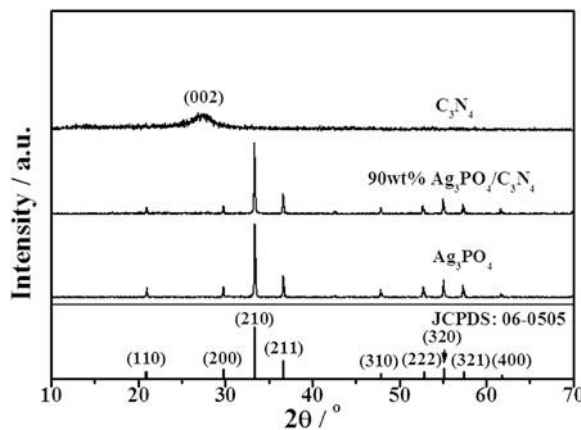


FIG. 1. XRD patterns of C_3N_4 , Ag_3PO_4 , and 90 wt% $\text{Ag}_3\text{PO}_4/\text{C}_3\text{N}_4$ composite.

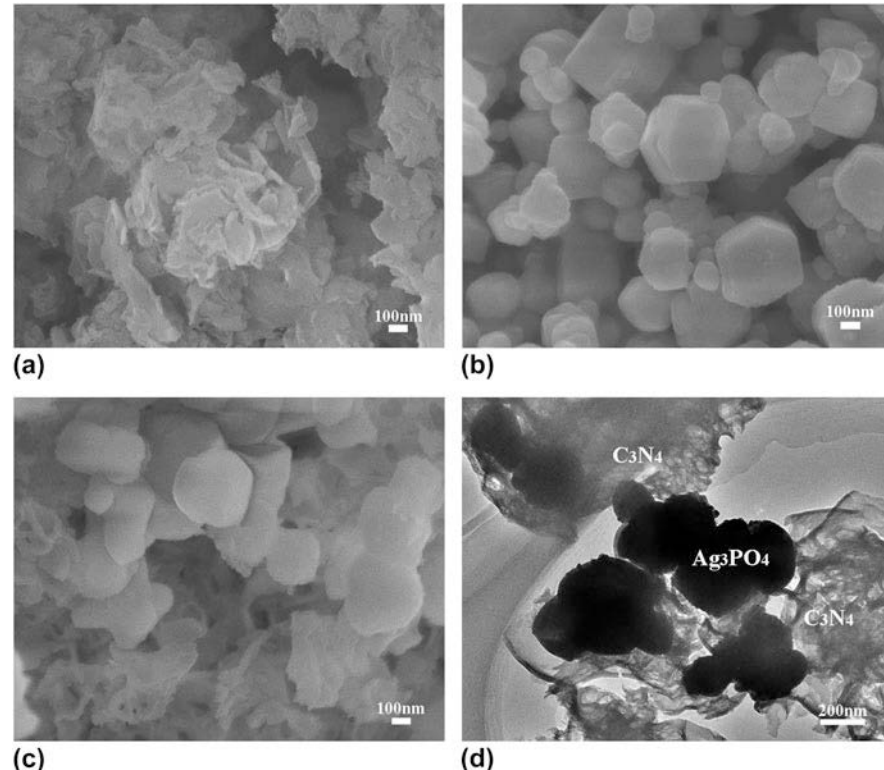


FIG. 2. FESEM images of C_3N_4 (a), Ag_3PO_4 (b), and 90 wt% $\text{Ag}_3\text{PO}_4/\text{C}_3\text{N}_4$ composite (c); TEM image of 90 wt% $\text{Ag}_3\text{PO}_4/\text{C}_3\text{N}_4$ composite (d).

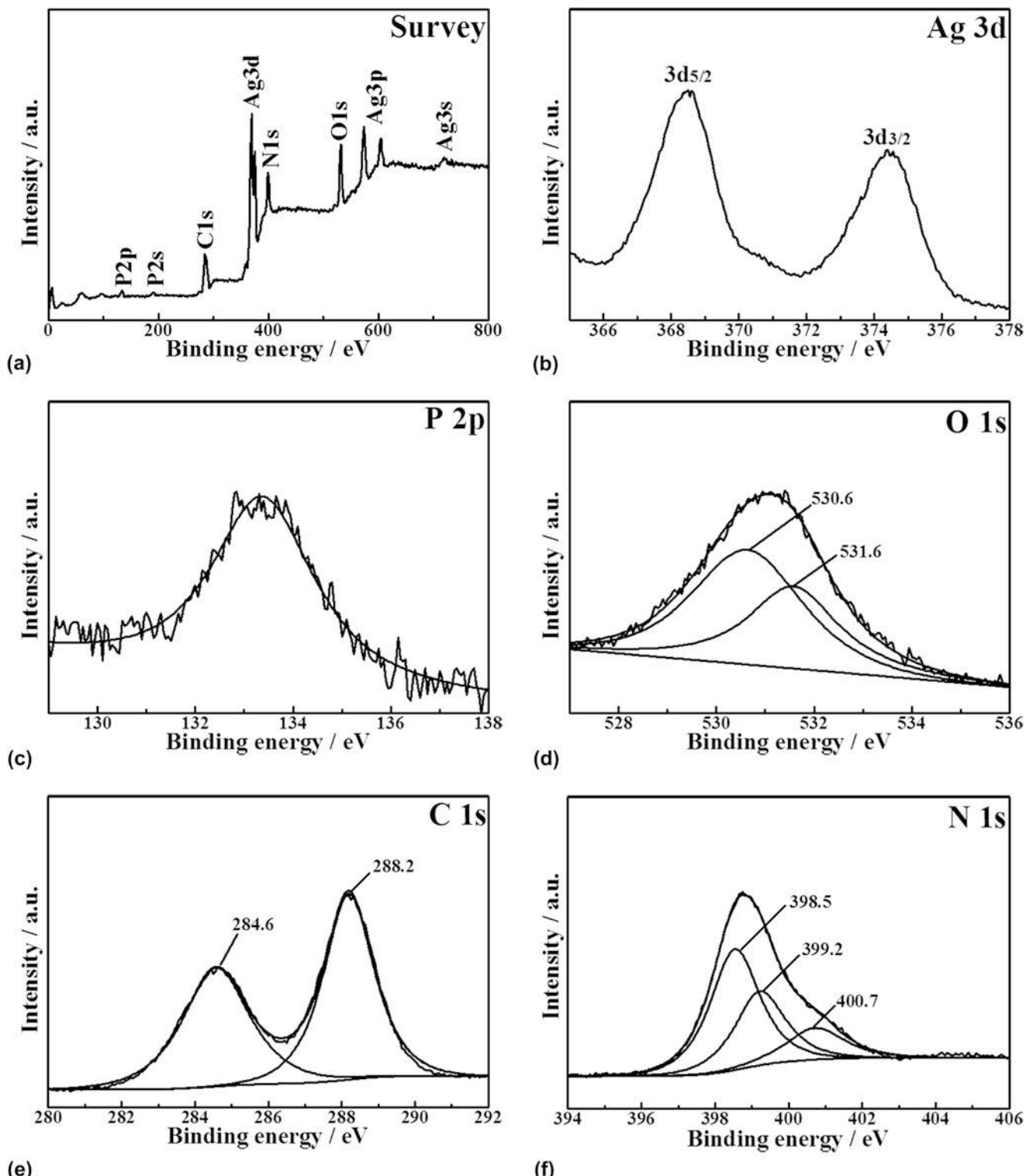


FIG. 3. XPS spectra of 90 wt% $\text{Ag}_3\text{PO}_4/\text{C}_3\text{N}_4$ composite: (a) XPS survey spectrum; (b) high resolution Ag 3d spectrum; (c) high resolution P 2p spectrum; (d) high resolution O 1s spectrum; (e) high resolution C 1s spectrum; and (f) high resolution N 1s spectrum.

399.2 eV correspond to sp^2 hybridized aromatic N bonded to carbon atoms ($\text{C}=\text{N}-\text{C}$) and the tertiary N bonded to carbon atoms in the form of $\text{N}-(\text{C})_3$ or $\text{H}-\text{N}-(\text{C})_2$, while the peak at 400.7 eV could be ascribed to

N–H side groups, which are consistent with the reported results on N 1s XPS spectra of C_3N_4 .²⁶ The XPS results verify the coexistence of Ag_3PO_4 and C_3N_4 in the composite.

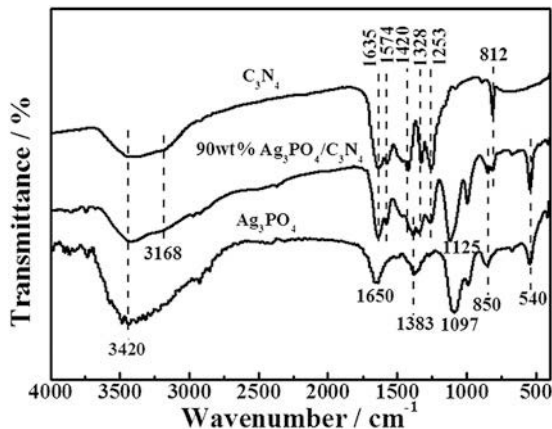


FIG. 4. FTIR spectra of C_3N_4 , Ag_3PO_4 , and 90 wt% $\text{Ag}_3\text{PO}_4/\text{C}_3\text{N}_4$ composite.

Figure 4 depicts the FTIR spectra of C_3N_4 , Ag_3PO_4 , and 90 wt% $\text{Ag}_3\text{PO}_4/\text{C}_3\text{N}_4$ composite. The broad peaks at about 3420 cm^{-1} in all of the spectra correspond to the stretching vibration mode of adsorbed H_2O molecules. As for bare C_3N_4 , the absorption band at 1635 cm^{-1} could be ascribed to $\text{C}=\text{N}$ stretching vibration modes, whereas the four peaks at 1253, 1328, 1420, and 1574 cm^{-1} are assigned to aromatic $\text{C}-\text{N}$ stretching. The peak at 812 cm^{-1} is related to the *s*-triazine ring. A shoulder band near 3168 cm^{-1} is attributed to the stretching modes of terminal $\text{N}-\text{H}$ groups.²⁶ In the case of Ag_3PO_4 , the peak at 1650 cm^{-1} is assigned to the $-\text{OH}$ bending vibration. The peak at around 540 cm^{-1} is ascribed to $\text{O}=\text{P}-\text{O}$ bending vibration, while the peaks at 850 and 1097 cm^{-1} are due to the symmetric and asymmetric stretching vibrations of $\text{P}-\text{O}-\text{P}$ rings. One band featured at 1383 cm^{-1} derives from the stretching vibration of doubly bonded oxygen ($\text{P}=\text{O}$) and the harmonics of the above modes.³³ For the 90 wt% $\text{Ag}_3\text{PO}_4/\text{C}_3\text{N}_4$ composite, the characteristic bands for Ag_3PO_4 and C_3N_4 coexist. In addition, the characteristic peak assigned to the stretching vibration of the $\text{P}-\text{O}-\text{P}$ group shifts to a higher wave number of 1125 cm^{-1} compared with that of 1097 cm^{-1} in bare Ag_3PO_4 , suggesting that the interaction between the Ag_3PO_4 and C_3N_4 has already appeared.³³ The interaction between Ag_3PO_4 and C_3N_4 may benefit the photogenerated charge carriers' transfer and then enhance the photocatalytic activity of composites.

Figure 5 shows the UV-vis DRS of C_3N_4 , Ag_3PO_4 , and 90 wt% $\text{Ag}_3\text{PO}_4/\text{C}_3\text{N}_4$ composite. As can be seen, single C_3N_4 and Ag_3PO_4 present the strong absorption edges at about 435 and 506 nm, which are attributed to the intrinsic band gap absorption. The band gaps of C_3N_4 and Ag_3PO_4 are estimated to be 2.85 and 2.45 eV according to the equation of $E_g = 1240/\lambda_g$, where E_g is the band gap energy of semiconductor and λ_g is the optical absorption edge of semiconductor. The 90 wt% $\text{Ag}_3\text{PO}_4/\text{C}_3\text{N}_4$ composite shows a combination of these two DRS contributing from Ag_3PO_4 and C_3N_4 .

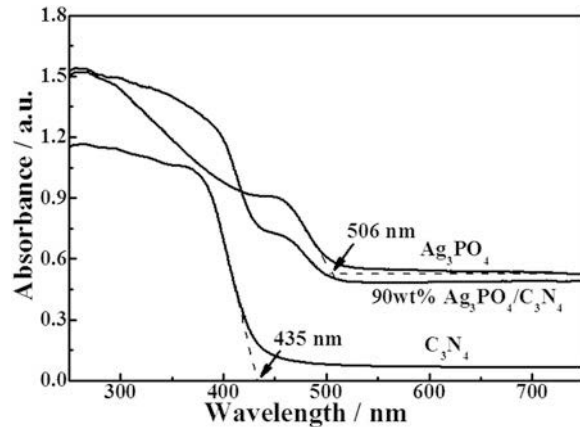


FIG. 5. UV-vis DRS of C_3N_4 , Ag_3PO_4 , and 90 wt% $\text{Ag}_3\text{PO}_4/\text{C}_3\text{N}_4$ composite.

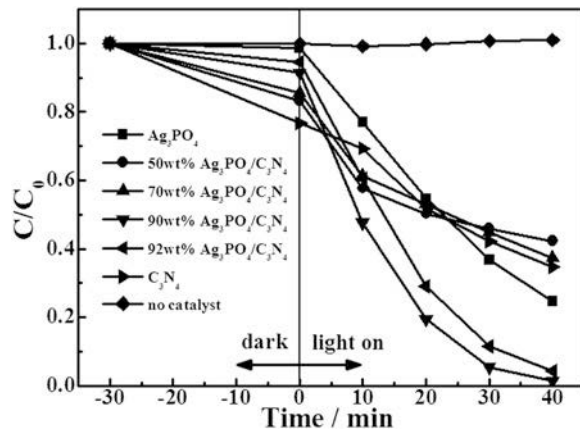


FIG. 6. Comparison of photocatalytic activities of samples for the degradation of RhB solution.

Figure 6 displays the photocatalytic activities of C_3N_4 , Ag_3PO_4 , and $\text{Ag}_3\text{PO}_4/\text{C}_3\text{N}_4$ composites with different mass ratios for the degradation of RhB solution. For comparison, the blank test was also conducted under the same reaction conditions. It can be seen that the degradation of RhB is negligible in the absence of photocatalysts under visible light irradiation for 40 min. Pristine Ag_3PO_4 exhibits better photocatalytic activity with the decolorization percentage of 75.4% after 40 min of visible light irradiation although it has a poor adsorption capacity. Bare C_3N_4 presents a best adsorption performance, and about 23.3% RhB molecules are adsorbed on its surface before illumination. Under visible light irradiation for 40 min, the decrease of RhB concentration reaches 65.3%. The adsorption abilities of $\text{Ag}_3\text{PO}_4/\text{C}_3\text{N}_4$ composites lie between Ag_3PO_4 and C_3N_4 . Moreover, the adsorption capacity declines with increasing the amount of Ag_3PO_4 in the composites. The decolorization percentages of RhB are about 57.7, 62.7, 98.5, and 95.7% for the 50, 70, 90, and 92 wt% $\text{Ag}_3\text{PO}_4/\text{C}_3\text{N}_4$ composites for 40 min visible light illumination,

respectively. As for a series of $\text{Ag}_3\text{PO}_4/\text{C}_3\text{N}_4$ photocatalysts, the photocatalytic activities of the composites improve with increasing the Ag_3PO_4 contents and the 90 wt% $\text{Ag}_3\text{PO}_4/\text{C}_3\text{N}_4$ composite shows the highest photocatalytic performance. Whereas further enhancing the amount of Ag_3PO_4 in the composites, the photocatalytic activity decreases, which is due to the excessive Ag_3PO_4 contents leading to the decrease of interfaces in the composites.

The photocatalytic degradation of RhB can be considered as a pseudo-first-order reaction with low concentration, and its kinetics can be expressed by the equation of $-\ln(C/C_0) = kt$, where k is the degradation rate constant, C_0 and C are the absorption equilibrium concentration of RhB and the concentration at a reaction time of t , respectively.³⁰ As shown in Fig. 7, the rate constants (k) of different samples are 0.03514, 0.01586, 0.01975, 0.10445, 0.07819, and 0.02080 min^{-1} for the pristine Ag_3PO_4 , 50, 70, 90, 92 wt% $\text{Ag}_3\text{PO}_4/\text{C}_3\text{N}_4$ composites, and C_3N_4 , respectively. For the degradation of RhB, the kinetic constant of 90 wt% $\text{Ag}_3\text{PO}_4/\text{C}_3\text{N}_4$ is about 3.0 and 5.0 times as large as those of pristine Ag_3PO_4 and C_3N_4 .

To test the stability of photocatalysts, the 90 wt% $\text{Ag}_3\text{PO}_4/\text{C}_3\text{N}_4$ composite was reused for photocatalytic reaction under the same conditions, and the result is shown in Fig. 8. The photocatalytic decolorization efficiency still reaches 90.8% after three runs of photodegradation of RhB, indicating that the composite has considerable photostability.

To investigate the reaction mechanism, isopropanol (IPA), triethanolamine (TEOA), and *p*-benzoquinone (BQ) were respectively introduced as the scavengers of hydroxyl radicals ($\cdot\text{OH}$), holes (h^+), and superoxide radicals ($\cdot\text{O}_2^-$) to examine the effects of reactive species on the photocatalytic degradation of RhB. The concentrations of IPA, TEOA, and BQ in the reaction system were 10, 10, and 1 $\text{mmol}\cdot\text{L}^{-1}$, respectively. From Fig. 9, it can be seen that the BQ and TEOA lead to an obvious suppression of the decolorization efficiency of RhB.

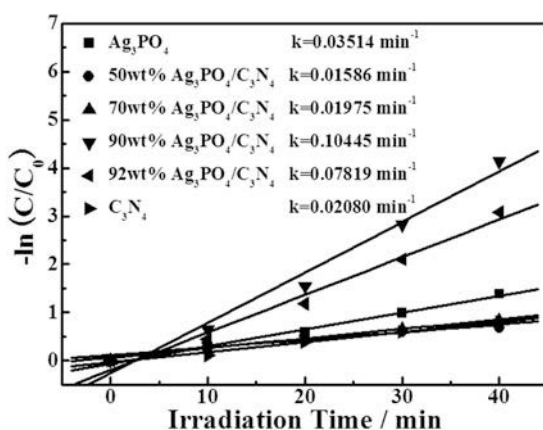


FIG. 7. Pseudo-first-order kinetics curves of RhB degradation over the different samples.

Whereas the IPA exhibits weakly restraining effect on the decolorization efficiency. The results suggest that h^+ and $\cdot\text{O}_2^-$ are the main active species for the degradation of RhB in the current system.

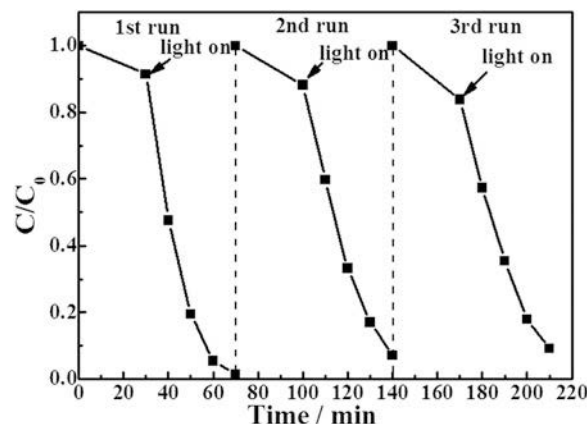


FIG. 8. Stability studies on photocatalytic degradation of RhB solution over 90 wt% $\text{Ag}_3\text{PO}_4/\text{C}_3\text{N}_4$ composite.

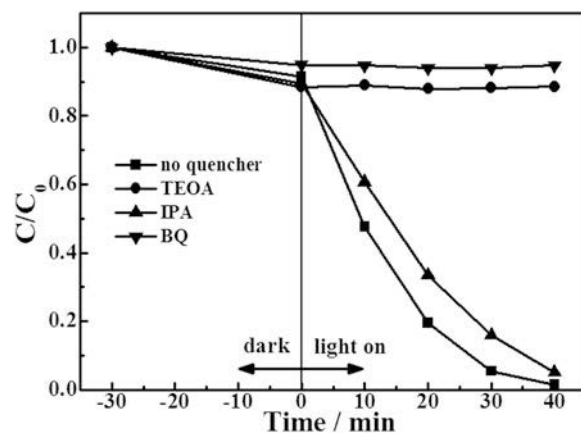


FIG. 9. The effect of reactive species on the photocatalytic degradation of RhB solution.

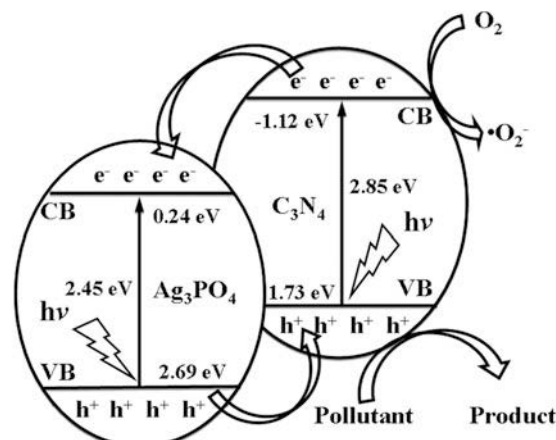


FIG. 10. The proposed mechanism of improved photocatalytic activity for the $\text{Ag}_3\text{PO}_4/\text{C}_3\text{N}_4$ composite.

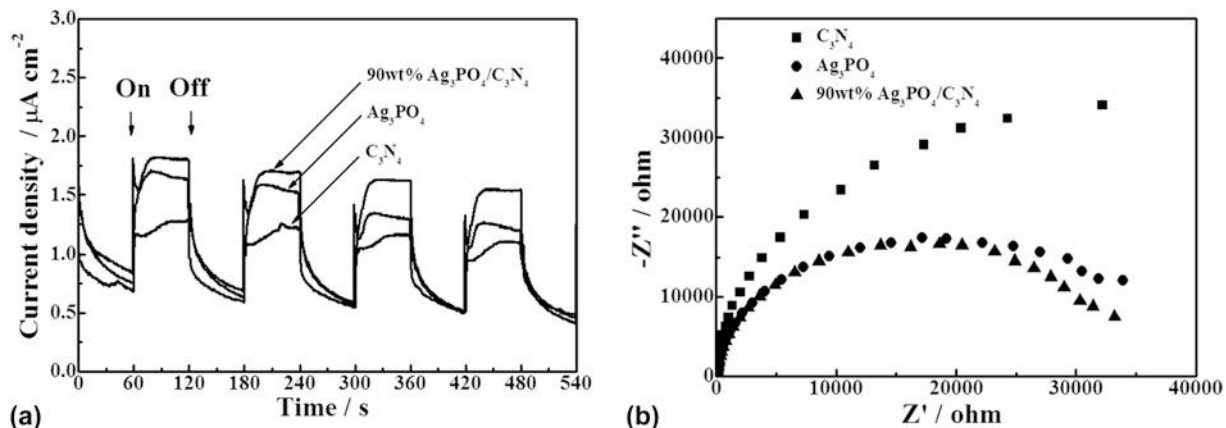


FIG. 11. Transient photocurrent responses (a) and EIS Nyquist plots (b) of Ag_3PO_4 , C_3N_4 , and 90 wt% $\text{Ag}_3\text{PO}_4/\text{C}_3\text{N}_4$ composite under visible light irradiation in $0.1 \text{ mol L}^{-1} \text{Na}_2\text{SO}_4$ solution.

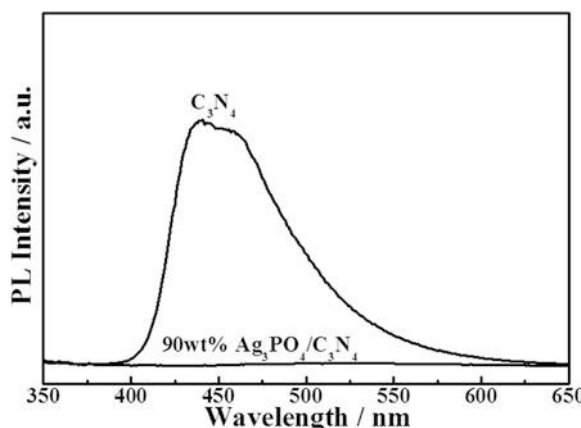


FIG. 12. PL emission spectra of C_3N_4 and 90 wt% $\text{Ag}_3\text{PO}_4/\text{C}_3\text{N}_4$ composite.

Based on the above results, a possible mechanism is proposed to explain the improvement of photocatalytic activity of $\text{Ag}_3\text{PO}_4/\text{C}_3\text{N}_4$ composite. As is well known, the efficient separation of photogenerated charge carriers is crucial for the enhancement of photocatalytic activity. As for the semiconductor composites, the migration direction of photogenerated charge carriers depends on the band edge potential positions. According to previous reports,^{25,26} the CB and VB potential of C_3N_4 are -1.12 and 1.73 eV, respectively (versus NHE), which are more negative than those of the CB (0.24 eV versus NHE) and VB (2.69 eV versus NHE) potentials of Ag_3PO_4 . This well-matched energy band structure facilitates the separation of charge carriers. As shown in Fig. 10, when the $\text{Ag}_3\text{PO}_4/\text{C}_3\text{N}_4$ composite is illuminated under visible light, both Ag_3PO_4 and C_3N_4 are excited to generate electron–hole pairs. The electrons in the CB of C_3N_4 can smoothly transfer into the CB of Ag_3PO_4 , meanwhile the holes in the VB of Ag_3PO_4 can conveniently migrate into the VB of C_3N_4 . As a result, the electron–hole pairs are efficiently separated between Ag_3PO_4 and C_3N_4 , which

benefits to improving the photocatalytic activity. Since the CB potential of Ag_3PO_4 is more positive than the single electron reduction potential of $\text{O}_2/\cdot\text{O}_2^-$ (-0.33 eV versus NHE),¹⁴ it cannot reduce O_2 to yield $\cdot\text{O}_2^-$ on the surface of Ag_3PO_4 . However, the photogenerated electrons from C_3N_4 can reduce the surface chemisorbed O_2 to give $\cdot\text{O}_2^-$ through one electron reaction. On the other hand, the VB potentials of Ag_3PO_4 and C_3N_4 are not more positive than the redox potentials of $\cdot\text{OH}/\text{H}_2\text{O}$ (2.72 eV versus NHE).¹⁴ This suggests that the photogenerated holes on the VB of Ag_3PO_4 and C_3N_4 could not react with H_2O to form $\cdot\text{OH}$. Consequently, the degradation of RhB would be the reaction with photogenerated holes directly.

To confirm the effective separation of photogenerated electrons and holes in the $\text{Ag}_3\text{PO}_4/\text{C}_3\text{N}_4$ composites, the transient photocurrent responses and electrochemical impedance spectroscopy (EIS) spectra have been used to investigate the interfacial charge separation efficiency over pure Ag_3PO_4 , C_3N_4 , and 90 wt% $\text{Ag}_3\text{PO}_4/\text{C}_3\text{N}_4$ composite. As shown in Fig. 11(a), the photocurrent density obtained over the 90 wt% $\text{Ag}_3\text{PO}_4/\text{C}_3\text{N}_4$ composite is obviously enhanced compared with that of pure Ag_3PO_4 and C_3N_4 . Photocurrent is formed mainly by transferring photogenerated electrons to the counter electrode; the higher photocurrent indicates more effective separation and longer lifetime of the photogenerated electrons on it. In addition, EIS Nyquist analysis was performed to study the interfacial electrons' transfer [Fig. 11(b)]. The diameter of the Nyquist circle of the 90 wt% $\text{Ag}_3\text{PO}_4/\text{C}_3\text{N}_4$ composite is smaller than that of single Ag_3PO_4 and C_3N_4 , suggesting that the 90 wt% $\text{Ag}_3\text{PO}_4/\text{C}_3\text{N}_4$ composite has a relatively lower charge transfer resistance at the contact interface between the electrode and electrolyte solution. This may prove that the 90 wt% $\text{Ag}_3\text{PO}_4/\text{C}_3\text{N}_4$ composite exhibits more efficient activity compared with pure Ag_3PO_4 and C_3N_4 .

The better separation of photogenerated electrons and holes in the $\text{Ag}_3\text{PO}_4/\text{C}_3\text{N}_4$ composite is also elucidated by PL emission spectra of single C_3N_4 and 90 wt%

$\text{Ag}_3\text{PO}_4/\text{C}_3\text{N}_4$ composite. It is well known that the PL signal of semiconductor material results from the recombination of photogenerated charge carriers. In generally, the lower PL intensity indicates the decrease in recombination rate of photogenerated charge carriers. As shown in Fig. 12, the main emission peak is centered at about 440 nm for the bare C_3N_4 , which is approximately equal to the band gap of C_3N_4 . In contrast, the quenching of PL peak is observed for the 90 wt% $\text{Ag}_3\text{PO}_4/\text{C}_3\text{N}_4$ composite. The result of PL verifies that the $\text{Ag}_3\text{PO}_4/\text{C}_3\text{N}_4$ composite can effectively separate photogenerated electron–hole pairs.

IV. CONCLUSIONS

In summary, the visible-light-responsive $\text{Ag}_3\text{PO}_4/\text{C}_3\text{N}_4$ composites were prepared by a facile in situ deposition of Ag_3PO_4 particles on the surface of C_3N_4 sheets and applied into photocatalytic degradation of RhB solution. The improved photocatalytic activity of $\text{Ag}_3\text{PO}_4/\text{C}_3\text{N}_4$ composites could be ascribed to the effective separation of photogenerated charge carriers. Photoelectrochemical and PL measurements confirmed the effective separation of photogenerated charges in the $\text{Ag}_3\text{PO}_4/\text{C}_3\text{N}_4$ composites. Moreover, the tests of radical scavengers indicated that h^+ and $\cdot\text{O}_2^-$ were the main active species for the degradation of RhB. The resultant $\text{Ag}_3\text{PO}_4/\text{C}_3\text{N}_4$ composites may be promising efficient photocatalysts for the degradation of organic pollutants in the industrial and engineering field.

ACKNOWLEDGMENT

This work was supported by Science and Technology Investigation Project of Educational Committee of Hubei Province, China (No. Q20141708).

REFERENCES

- X.L. Hu, G.S. Li, and J.C. Yu: Design, fabrication, and modification of nanostructured semiconductor materials for environmental and energy applications. *Langmuir* **26**, 3031 (2010).
- A. Kubacka, M. Fernández-García, and G. Colón: Advanced nanoarchitectures for solar photocatalytic applications. *Chem. Rev.* **112**, 1555 (2012).
- Y. Sang, L. Kuai, C.Y. Chen, Z. Fang, and B.Y. Geng: Fabrication of a visible-light-driven plasmonic photocatalyst of $\text{AgVO}_3@\text{AgBr}@\text{Ag}$ nanobelt heterostructures. *ACS Appl. Mater. Interfaces* **6**, 5061 (2014).
- G.C. Xi and J.H. Ye: Synthesis of bismuth vanadate nanoplates with exposed {001} facets and enhanced visible-light photocatalytic properties. *Chem. Commun.* **46**, 1893 (2010).
- J.J. Wu, F.Q. Huang, X.J. Lü, P. Chen, D.Y. Wan, and F.F. Xu: Improved visible-light photocatalysis of nano- $\text{Bi}_2\text{Sn}_2\text{O}_7$ with dispersed s-bands. *J. Mater. Chem.* **21**, 3872 (2011).
- Y.P. Bi, S.X. Ouyang, N. Umezawa, J.Y. Cao, and J.H. Ye: Facet effect of single-crystalline Ag_3PO_4 sub-microcrystals on photocatalytic properties. *J. Am. Chem. Soc.* **133**, 6490 (2011).
- W.G. Wang, B. Cheng, J.G. Yu, G. Liu, and W.H. Fan: Visible-light photocatalytic activity and deactivation mechanism of Ag_3PO_4 spherical particles. *Chem. Asian J.* **7**, 1902 (2012).
- H. Wang, L. He, L.H. Wang, P.F. Hu, L. Guo, X.D. Han, and J.H. Li: Facile synthesis of Ag_3PO_4 tetrapod microcrystals with an increased percentage of exposed {110} facets and highly efficient photocatalytic properties. *CrystEngComm* **14**, 8342 (2012).
- Y.J. Cui, J.H. Huang, X.Z. Fu, and X.C. Wang: Metal-free photocatalytic degradation of 4-chlorophenol in water by mesoporous carbon nitride semiconductors. *Catal. Sci. Technol.* **2**, 1396 (2012).
- J.H. Liu, T.K. Zhang, Z.C. Wang, G. Dawson, and W. Chen: Simple pyrolysis of urea into graphitic carbon nitride with recyclable adsorption and photocatalytic activity. *J. Mater. Chem.* **21**, 14398 (2011).
- P.Y. Dong, Y.H. Wang, B.C. Cao, S.Y. Xin, L.N. Guo, J. Zhang, and F.H. Li: Ag_3PO_4 /reduced graphite oxide sheets nanocomposites with highly enhanced visible light photocatalytic activity and stability. *Appl. Catal., B* **132–133**, 45 (2013).
- Z. Wang, L. Yin, M. Zhang, G.W. Zhou, H. Fei, H.X. Shi, and H.J. Dai: Synthesis and characterization of Ag_3PO_4 /multiwalled carbon nanotube composite photocatalyst with enhanced photocatalytic activity and stability under visible light. *J. Mater. Sci.* **49**, 1585 (2014).
- J.X. Sun, Y.P. Yuan, L.G. Qiu, X. Jiang, A.J. Xie, Y.H. Shen, and J.F. Zhu: Fabrication of composite photocatalyst $\text{g-C}_3\text{N}_4\text{-ZnO}$ and enhancement of photocatalytic activity under visible light. *Dalton Trans.* **41**, 6756 (2012).
- J. Cao, B.D. Luo, H.L. Lin, B.Y. Xu, and S.F. Chen: Visible light photocatalytic activity enhancement and mechanism of $\text{AgBr}/\text{Ag}_3\text{PO}_4$ hybrids for degradation of methyl orange. *J. Hazard. Mater.* **217–218**, 107 (2012).
- W.F. Yao, B. Zhang, C.P. Huang, C. Ma, X.L. Song, and Q.J. Xu: Synthesis and characterization of high efficiency and stable $\text{Ag}_3\text{PO}_4/\text{TiO}_2$ visible light photocatalyst for the degradation of methylene blue and rhodamine B solutions. *J. Mater. Chem.* **22**, 4050 (2012).
- W. Liu, M.L. Wang, C.X. Xu, S.F. Chen, and X.L. Fu: $\text{Ag}_3\text{PO}_4/\text{ZnO}$: An efficient visible-light-sensitized composite with its application in photocatalytic degradation of rhodamine B. *Mater. Res. Bull.* **48**, 106 (2013).
- L.L. Zhang, H.C. Zhang, H. Huang, Y. Liu, and Z.H. Kang: $\text{Ag}_3\text{PO}_4/\text{SnO}_2$ semiconductor nanocomposites with enhanced photocatalytic activity and stability. *New J. Chem.* **36**, 1541 (2012).
- Y.S. Xu and W.D. Zhang: Monodispersed Ag_3PO_4 nanocrystals loaded on the surface of spherical Bi_2MoO_6 with enhanced photocatalytic performance. *Dalton Trans.* **42**, 1094 (2013).
- G.K. Fu, G.N. Xu, S.P. Chen, L. Lei, and M.L. Zhang: $\text{Ag}_3\text{PO}_4/\text{Bi}_2\text{WO}_6$ hierarchical heterostructures with enhanced visible light photocatalytic activity for the degradation of phenol. *Catal. Commun.* **40**, 120 (2013).
- B. Chai, T.Y. Peng, J. Mao, K. Li, and L. Zan: Graphitic carbon nitride ($\text{g-C}_3\text{N}_4$)-Pt-TiO₂ nanocomposite as an efficient photocatalyst for hydrogen production under visible light irradiation. *Phys. Chem. Chem. Phys.* **14**, 16745 (2012).
- Y.J. Wang, R. Shi, J. Lin, and Y.F. Zhu: Enhancement of photocurrent and photocatalytic activity of ZnO hybridized with graphite-like C_3N_4 . *Energy Environ. Sci.* **4**, 2922 (2011).
- L.M. Sun, X. Zhao, C.J. Jia, Y.X. Zhou, X.F. Cheng, P. Li, L. Liu, and W.L. Fan: Enhanced visible-light photocatalytic activity of $\text{g-C}_3\text{N}_4\text{-ZnWO}_4$ by fabricating a heterojunction: Investigation based on experimental and theoretical studies. *J. Mater. Chem.* **22**, 23428 (2012).
- J. Fu, B.B. Chang, Y.L. Tian, F.N. Xi, and X.P. Dong: Novel $\text{C}_3\text{N}_4\text{-CdS}$ composite photocatalysts with organic-inorganic heterojunctions: *In situ* synthesis exceptional activity, high stability and photocatalytic mechanism. *J. Mater. Chem. A* **1**, 3083 (2013).
- L.Q. Ye, J.Y. Liu, Z. Jiang, T.Y. Peng, and L. Zan: Facets coupling of $\text{BiOBr-g-C}_3\text{N}_4$ composite photocatalyst for enhanced

- visible-light-driven photocatalytic activity. *Appl. Catal., B* **142–143**, 1 (2013).
25. H. Katsumata, T. Sakai, T. Suzuki, and S. Kaneko: Highly efficient photocatalytic activity of $\text{g-C}_3\text{N}_4/\text{Ag}_3\text{PO}_4$ hybrid photocatalysts through Z-scheme photocatalytic mechanism under visible light. *Ind. Eng. Chem. Res.* **53**, 8018 (2014).
26. B. Chai, X. Liao, F.K. Song, and H. Zhou: Fullerene modified C_3N_4 composites with enhanced photocatalytic activity under visible light irradiation. *Dalton Trans.* **43**, 982 (2014).
27. Z.L. Xiu, H. Bo, Y.Z. Wu, and X.P. Hao: Graphite-like C_3N_4 modified Ag_3PO_4 nanoparticles with highly enhanced photocatalytic activities under visible light irradiation. *Appl. Surf. Sci.* **289**, 394 (2014).
28. S. Kumar, T. Surendar, A. Baruah, and V. Shanker: Synthesis of a novel and stable $\text{g-C}_3\text{N}_4\text{-Ag}_3\text{PO}_4$ hybrid nanocomposite photocatalyst and study of the photocatalytic activity under visible light irradiation. *J. Mater. Chem. A* **1**, 5333 (2013).
29. D.L. Jiang, J.J. Zhu, M. Chen, and J.M. Xie: Highly efficient heterojunction photocatalyst based on nanoporous $\text{g-C}_3\text{N}_4$ sheets modified by Ag_3PO_4 nanoparticles: Synthesis and enhanced photocatalytic activity. *J. Colloid Interface Sci.* **417**, 115 (2014).
30. F.J. Zhang, F.Z. Xie, S.F. Zhu, J. Liu, J. Zhang, S.F. Mei, and W. Zhao: A novel photofunctional $\text{g-C}_3\text{N}_4/\text{Ag}_3\text{PO}_4$ bulk heterojunction for decolorization of Rh.B. *Chem. Eng. J.* **228**, 435 (2013).
31. P.Z. He, L.M. Song, S.J. Zhang, X.Q. Wu, and Q.W. Wei: Synthesis of $\text{g-C}_3\text{N}_4/\text{Ag}_3\text{PO}_4$ heterojunction with enhanced photocatalytic performance. *Mater. Res. Bull.* **51**, 432 (2014).
32. M. Ge, N. Zhu, Y.P. Zhao, J. Li, and L. Liu: Sunlight-assisted degradation of dye pollutants in Ag_3PO_4 suspension. *Ind. Eng. Chem. Res.* **51**, 5167 (2012).
33. Q.H. Liang, Y. Shi, W.J. Ma, Z. Li, and X.M. Yang: Enhanced photocatalytic activity and structural stability by hybridizing Ag_3PO_4 nanospheres with graphene oxide sheets. *Phys. Chem. Chem. Phys.* **14**, 15657 (2012).